Available online at www.sciencedirect.com
SCIENCE DIRECT®
PERGAMON
International Journal of Heat and Mass Transfer 46 (2003) 3831–3840
International Journal of HEAT and MASS TRANSFER
www.elsevier.com/locate/ijhmt

Convection in a vertical cavity submitted to crossed uniform heat fluxes

Michel Prud'homme *, Habiba Bougherara, Ali Bahloul

Department of Mechanical Engineering, École Polytechnique de Montréal, C.P. 6079, Succ. Centre-ville, Montréal, Québec, Canada H3C 3A7

Received 7 September 2002; received in revised form 28 March 2003

Abstract

In this study, free convection in a vertical cavity heated from the four walls by uniform heat fluxes is considered. Analytical solutions are derived for a fully developed base flow, for which linear stability analysis predicts the growth of oblique, three-dimensional disturbances in general. A Hopf type bifurcation occurs at the critical Rayleigh number, over the entire range of Prandtl numbers and heat flux ratios considered, characterized by oscillating instabilities. Depending mostly on the value of the Prandtl number, either thermal, for $Pr > 1$, or hydrodynamic, for $Pr < 1$, instability modes are predicted. For small Prandtl numbers, both modes can occur at the codimension two intersection points of the critical branches.

1. Introduction

The possibility of obtaining parallel flow patterns has been reported many times in the litterature on the classical problem of natural convection in a rectangular enclosure. Bejan [1], for instance, described a parallel flow region in a thin, vertical, fluid saturated, porous cavity insulated on the sides and heated from the top by a constant flux. In the case of shallow cavities filled with a fluid, this time, the works of Cormack et al. [2,3] as well as Imberger [4] and Bejan and Tien [5] also mentioned the existence of parallel flow in convection when different temperatures were imposed on the sides of the cavity and the top and bottom were kept insulated.

It is well known, both theoretically and experimentally, that the parallel flows mentioned above may become unstable at high Reynolds numbers. In general, the critical value for the onset of the flow instability regime is strongly dependent on the boundary conditions imposed on the walls of the enclosure, as described in the works of Kassoy and Cotte [6], Wang et al. [7] and those of Vasseur et al. [8], Sen et al. [9] for an inclined cavity. In a slightly different context, Nield [10] showed that different instability regimes, in a shallow porous saturated layer submitted to an oblique temperature gradient, could be obtained by varying the vertical to lateral temperature gradient ratio. Kimura et al. [11] considered the stability problem for a porous medium in the same geometry as Nield, but this time for insulated vertical boundaries and a constant heat flux applied from below. They found a critical transition from the steady parallel base flow to an oscillatory instability regime.

For a fluid medium, Korpela et al. [12] determined that the instability in a vertical cavity with a fixed temperature difference on the sides is either of hydrodynamic or thermal origin depending on the Prandtl number. They established that the critical modes are hydrodynamic and stationary if $Pr < 12.7$ and thermal and oscillatory if $Pr > 12.7$. The analysis was extended by Bergholz [13] to a wide range of Prandtl numbers and levels of stratification of the base flow. His work showed that transition from stationary to oscillatory modes occurs with increasing stratification at small Prandtl numbers, and from oscillatory to stationary at large Prandtl numbers. Suslov and Paolucci [14] also examined

* Corresponding author. Tel.: +1-514-370-4711/4507; fax: +1-514-370-5917.
E-mail address: miprud@meca.polymtl.ca (M. Prud'homme).

0017-9310/03/$ - see front matter © 2003 Elsevier Ltd. All rights reserved.
doi:10.1016/S0017-9310(03)00192-3

Nomenclature

A	aspect ratio
C	constant
D	derivative operator
d	distance between the walls
F	factor
g	gravity
$\hat{\mathbf{g}}$	unit vector
H	height
k	vertical wavenumber
k_T	thermal concuctivity
L	operator
l	transverse wavenumber
N	number of grid points
p	pressure
Pr	Prandtl number
Q	transverse heat flux
q	heat flux ratio
Ra	Rayleigh number
Re	real part
t	time
T	temperature
$\mathbf{u}$	velocity vector
u, v, w	velocity components
x, y, z	coordinates

Greek symbols

α	stratification parameter
α_T	thermal diffusivity
β_T	coefficient of thermal expansion
β	direction of propagation
γ	parameter
Δ	increment
θ	base flow temperature profile
ν	kinematic viscosity
ρ	density
σ	complex amplification rate
ψ	base flow stream function
ω	oscillation frequency

Superscripts

$\sim$	disturbance quantity, 3-D
$\wedge$	disturbance quantity, 1-D

Subscripts

c	critical value
i	imaginary part
r	real part
0	reference value

Other symbols

D/Dt	material derivative
$\|\|$	modulus
∇	gradient
∇^2	laplacian

flow instability in a vertical cavity with a fixed temperature difference on the sides, but under non-Boussinesq conditions and no stratification of the base flow temperature field. They reported, assuming the transport properties of air for the active fluid, two modes of oscillatory instabilities: a shear-driven one for the smaller temperature differences and a buoyancy-driven one for the larger temperature differences.

For a cylindrical annulus with the inner and outer walls maintained at different temperatures, Bahloul et al. [15] showed the existence of oscillatory thermal and hydrodynamic oscillatory modes. They found that in the limiting case of a radius ratio tending to 1, i.e. vertical parallel walls, the hydrodynamic mode becomes stationary, in agreement with the findings of the authors above [12,13].

Even though natural convection generated within a cavity by a given heat flux can be encountered in many types of configurations, in such diverse contexts as geophysics problems or the conception of electrochemical systems, nearly adiabatic conditions on the rest of the boundary do not always occur in practice. This problem has received little attention so far. The purpose of the present study is then to perform a stability analysis for a fluid in a vertical cavity heated by crossed uniform heat fluxes, of different magnitudes, on the horizontal and vertical walls, as sketched in Fig. 1, and to determine the critical parameters dependence on the Prandtl number and heat flux ratio q. Analytical solu-

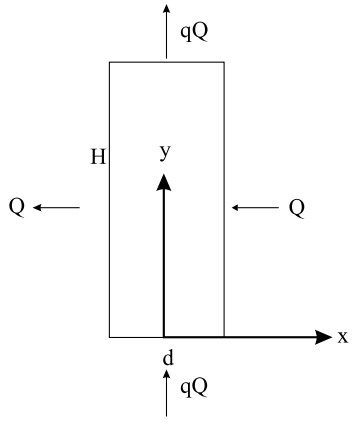

Fig. 1. Geometry and boundary conditions.

tions for the base flow stream function and temperature field are first derived within the parallel flow approximation, and validated against numerical simulations. Linear stability equations are then solved to determine critical parameter values at different Prandtl numbers and heat flux ratios.

2. Problem definition

Stability of free convection flow is examined within a tall and deep enclosure as in Fig. 1, with adiabatic walls in the normal direction and heated by crossed fluxes on the remaining walls, as sketched. It is assumed from the start that the temperature differences are small enough for Boussinesq conditions to prevail [16]. For convection taking place in a newtonian, incompressible fluid of constant kinematic viscosity v, thermal diffusivity α_T and coefficient of thermal expansion β_T, length, temperature, velocity and time can be scaled according to

$$d, \quad \Delta T = \frac{Qd}{k_T}, \quad \frac{\alpha_T}{d}, \quad \frac{d^2}{\alpha_T} \tag{1}$$

where all properties are evaluated at some reference temperature T_0. Using the standard Boussinesq approximation for the density $\rho = \rho_0[1 - \beta_T(T - T_0)]$ in the body force, the dimensionless governing equations of the problem become

$$\nabla \cdot \vec{\mathbf{u}} = 0 \tag{2}$$

$$\frac{\mathrm{D}}{\mathrm{D}t}\vec{\mathbf{u}} = -\nabla p + Pr\nabla^2\vec{\mathbf{u}} - Ra\,Pr\,T\hat{\mathbf{g}} \tag{3}$$

$$\frac{\mathrm{D}T}{\mathrm{D}t} = \nabla^2 T \tag{4}$$

in terms of the Prandtl number $Pr = v/\alpha_T$ and the Rayleigh number $Ra = g\beta_T\Delta T d^3/v\alpha_T$.

3. Base flow

For sufficiently large values of the aspect ratio A, fully developed flow conditions are possible in the central part of the cavity, with streamlines nearly parallel with the y axis, as shown in Fig. 2 for $Ra = 10^5$ and $q = 0$ as well as $q = 3$. The extent of the parallel flow region within the cavity is not as large for $q = 3$ as for $q = 0$ however, so that one would normally expect that aspect ratios $A > 5$ are required in order to make the parallel flow approximation for larger values of q.

When the approximation is valid, the base flow can be described from a stream function of the form $\psi = \psi(x)$ only. The continuity equation (2) is then automatically verified, while the momentum equation (3) reduces to

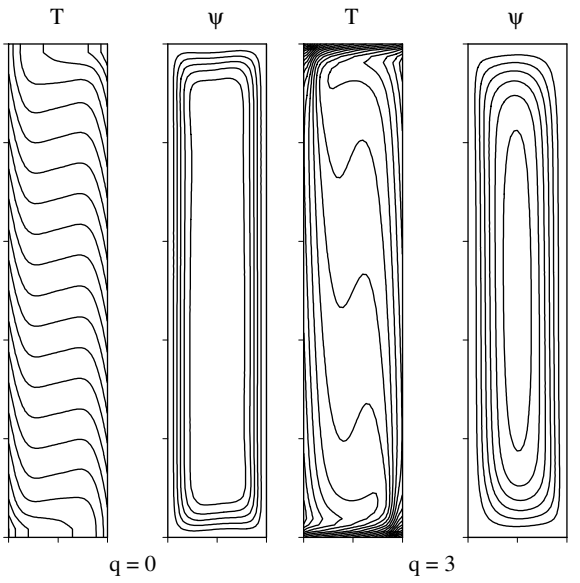

Fig. 2. Flow in a finite cavity, $Ra = 10^5$ and $A = 5$.

$$\psi'''' - Ra\frac{\partial T}{\partial x} = 0 \tag{5}$$

with boundary conditions $\psi = \psi' = 0$, $x = \pm 1/2$. Differentiating Eq. (5) with respect to y shows that the temperature profile must have the form $T = \theta(x) + g(y)$. It follows next from the temperature equation (4) that $g(y)$ must be linear in y in order to avoid trivial solutions for the stream function. The temperature field, up to an additive constant, is therefore given by

$$T = \theta(x) + \alpha y \tag{6}$$

where α is the vertical temperature gradient, with $\alpha > 0$ for stable stratification, while θ must satisfy the boundary condition $\theta' = 1$, $x = \pm 1/2$. The temperature equation may then be integrated once to get

$$\theta'(x) = -\alpha\psi + 1 \tag{7}$$

Eliminating now T from Eq. (5) using Eqs. (6) and (7) leads to an equation in terms of Ψ only

$$\psi'''' + \alpha Ra\psi = Ra \tag{8}$$

The solution of Eq. (8) above is given by

$$\psi(x) = \frac{1}{\alpha}\mathrm{Re}\{C\cosh(\lambda x) + 1\} \tag{9}$$

where λ and $C(\gamma)$ are complex quantities, defined respectively from $\lambda = \gamma(1 + i)$, where $4\gamma^4 = \alpha Ra$ and

$$C = \frac{2\lambda^*\sinh(\lambda^*/2)}{\gamma i[\sinh(\gamma) + \sin(\gamma)]} \tag{10}$$

For a given value of α, the solution for $\theta(x)$ is found at once from Eqs. (7) and (9) as

$$\theta(x) = -\mathrm{Re}\left\{\frac{C}{\lambda}\sinh(\lambda x)\right\} \tag{11}$$

For the crossed flux heating considered here, the vertical temperature gradient is not an independent parameter, as it was under the set of boundary conditions prescribed in the study of Bergholz [13]. It cannot be specified a priori, but must be determined instead for given values of Ra and q, from thermal energy conservation requirements, as follows. The temperature equation (4) in conservative form has to be integrated over an arbitrary section of the cavity in the first place. Using then the divergence theorem, Eq. (6) and the boundary condition $\partial T/\partial y = -q$ at $y = 0$ leads to

$$\int_{-1/2}^{1/2}\left(\frac{\partial\psi}{\partial x}T + \frac{\partial T}{\partial y}\right)\mathrm{d}x = -q \tag{12}$$

The left-hand side of Eq. (12) may be evaluated using Eqs. (9) and (11) to obtain for α the transcendental equation

$$\begin{aligned}&\alpha^2 + \alpha q + D(\gamma) = 0\\ &D(\gamma) = \frac{\mathrm{Re}}{4}\left\{C^2\left(1 - \frac{\sinh(\lambda)}{\lambda}\right)\right\}\end{aligned} \tag{13}$$

Solutions of Eq. (13) for heat flux ratio values $q = 0$, 1, 3 are presented in Fig. 3. It is seen that the stratification parameter α is negative at first for small Rayleigh numbers and subsequently becomes positive for all the larger values of Ra afterwards. Let us mention briefly that multiple parallel flow solutions for unstable stratification with $\alpha < 0$ may also exist at a given Rayleigh number. The dashed and dotted plots for $q = 3$ shown on the figure, for illustrative purposes only, correspond to such solutions, which are confined to a certain range of Rayleigh numbers. Each represents either a bicellular natural or antinatural pattern or a unicellular antinatural pattern, and we shall consider only the base flow solution with $\alpha > 0$ for the stability analysis.

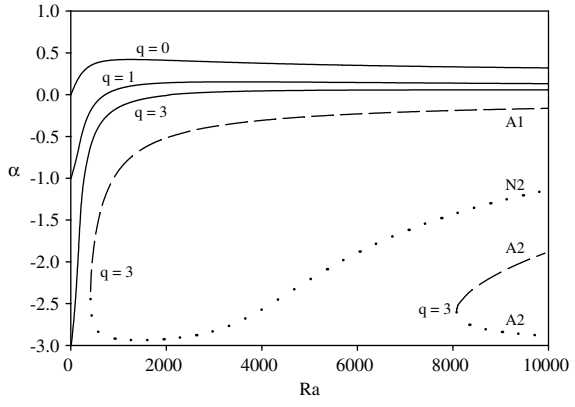

Fig. 3. Stratification parameter α vs Ra. A1: antinatural, 1 cell; A2: antinatural, 2 cells; N2: natural, 2 cells.

It is instructive at this point to consider the behavior of $D(\gamma)$ in Eq. (13) in the limiting cases of small and large values of γ. Expanding D in powers of γ shows that $D \approx -\alpha Ra/720$ to leading order, as α gets close to zero. Thus, stable stratification occurs only when $Ra > 720q$. For large Rayleigh numbers, boundary layer are formed at the vertical walls and some simplifications can be made in the model. When γ is greater than 5.0 or so, it is possible to make first the approximation $C \approx 2^{3/2}\exp(-\lambda/2 - 3\pi i/4)$ in Eq. (10) and $D \approx -1/2\gamma$ for $\alpha > 0$ in Eq. (13), which then simplifies to

$$\alpha^{9/4} + \alpha^{5/4}q - (4Ra)^{-1/4} = 0 \tag{14}$$

Table 1 compares the values of the stratification parameter obtained from Eqs. (13) and (14). It is clear from the data that both forms are nearly equivalent for $Ra = 10^5$ and beyond. For the sake of completeness, the boundary layer counterparts of the base flow solutions Eqs. (9) and (11) are given below as

$$\begin{aligned}\psi(x) &= \frac{1}{\alpha}\{f_1(x) + f_{-1}(x)\};\\ f_\xi(x) &= \sqrt{2}\exp[\gamma(\xi x - 1/2)]\cos[\gamma(\xi x - 1/2) - 3\pi/4] + 1/2\\ \theta(x) &= \frac{1}{\gamma}\{g_1(x) - g_{-1}(x)\};\\ g_\xi(x) &= \exp[\gamma(\xi x - 1/2)]\cos[\gamma(\xi x - 1/2)]\end{aligned} \tag{15}$$

where the contributions of the right- and left-hand side boundary are referred to by $\xi = 1$ and -1, respectively.

4. Linear stability analysis

Let small amplitude perturbations of the temperature, pressure, and velocity field components of the form

$$\tilde{f} = \mathrm{Re}\{\hat{f}(x)\exp[\sigma t + i(ky + lz)]\} \tag{16}$$

be added to the base flow, where $\hat{f}$ is a complex quantity, k and l are the real vertical and transverse wave-

Table 1
Base flow parameters, $q = 3$, exact and boundary layer values

Ra	α exact	α boundary layer	γ exact	γ boundary layer
2.5×10^4	4.974×10^{-2}	4.108×10^{-2}	4.200	4.003
5.0×10^4	4.098×10^{-2}	3.581×10^{-2}	4.757	4.600
1.0×10^5	3.323×10^{-2}	3.121×10^{-2}	5.369	5.285
2.0×10^5	2.736×10^{-2}	2.712×10^{-2}	6.082	6.073
4.0×10^5	2.334×10^{-2}	2.370×10^{-2}	6.951	6.977

numbers, respectively, and $\sigma = \sigma_r + i\sigma_i$ is the complex amplification rate. The wavenumber vector components are assumed real, as it is customary for temporal stability analysis. Substitution of the sum of the base flow and perturbation variables, into the set of governing equations (2)–(4), followed by linearization to first-order in small quantities, yields the system of equations

$$\begin{aligned}
&D\hat{u} + ik\hat{v} + il\hat{w} = 0\\
&(F - PrL)\hat{u} = -D\hat{p}\\
&(F - PrL)\hat{v} = -ik\hat{p} + \psi''\hat{u} + RaPr\hat{T}\\
&(F - PrL)\hat{w} = -il\hat{p}\\
&(F - L)\hat{T} = -\theta'\hat{u} - \alpha\hat{v}
\end{aligned} \tag{17}$$

in which D is simply equal to d/dx and $F = \sigma - ik\psi'$, while L stands for the operator $D^2 - k^2 - l^2$. This set of equations, together with the boundary conditions $\hat{u}' = \hat{u} = \hat{v} = \hat{w} = \hat{T}' = 0$ at $x = \pm 1/2$, defines an eigenvalue problem in σ for a set of given parameter values Ra, Pr, q, k and l.

It is clear from Eq. (17) that the velocity field becomes uncoupled from temperature when $\hat{v}$ vanishes, so that the only possible two-dimensional instability that could occur is the one resulting from a disturbance in which $l = 0$. Unfortunately, unless $\alpha = 0$, Squire's transformation (see, for instance, Drazin and Reid [18]) cannot be used here to formally reduce the three-dimensional stability problem to an equivalent two-dimensional one. We must deal therefore with the full three-dimensional stability problem. Let us first eliminate $\hat{p}$ and $\hat{w}$ from Eq. (17) using the continuity and transverse momentum equations and rewrite the problem in matrix form

$$\begin{bmatrix} PrL^2 + ik(\psi'L - \psi''') & 0 & -ikRaPrD \\ k(k\psi' - iPrL)D + l^2\psi'' & \tilde{k}^2(ik\psi' + PrL) & l^2RaPr \\ -\theta' & -\alpha & L + ik\psi' \end{bmatrix} \times \begin{Bmatrix} \hat{u} \\ \hat{v} \\ \hat{T} \end{Bmatrix} = \sigma \begin{bmatrix} L & 0 & 0 \\ -ikD & \tilde{k}^2 & 0 \\ 0 & 0 & 1 \end{bmatrix} \begin{Bmatrix} \hat{u} \\ \hat{v} \\ \hat{T} \end{Bmatrix} \tag{18}$$

where $\tilde{k}^2 = k^2 + l^2$ is simply the modulus of the wavenumber vector. Solution of Eq. (18) can be achieved in several ways. One of the most straightforward is to solve the equations by finite-differences. Five-point central schemes are used for the velocity equations, allowing fourth-order accuracy for the first and second derivatives and second-order accuracy for the higher derivatives. The standard, three-point, second-order scheme is employed for the temperature equation. Neuman-type boundary conditions for the velocity and temperature perturbation are discretized using forward and backward difference formulas of the fourth and second order, respectively.

For N computational points, the resulting discrete system has $3N$ eigenvalues that can be found using a standard IMSL subroutine such as DGVCCG. The value of Ra for which the maximal growth rate σ_r among the $3N$ eigenvalues cancels is determined iteratively by Newton's method, holding q, k, l, Pr constant. Repeating the procedure for different wavenumbers k or l determines a marginal stability surface for the given values of q and Pr. The minimum value of Ra over the stability surface corresponds to the critical Rayleigh number $Ra_c(q, Pr)$.

Using finite-difference schemes to solve the eigenvalue problem requires a larger number of computational points to obtain accurate results than, say, Chebyshev or spectral methods. The computational time needed to achieve convergence remains quite reasonable however. It is instructive to validate our approach by trying to duplicate the results obtained by Bergholz with Galerkin's method. Let us mention that the eigenvalue equations in Bergholz's case are the same as ours in Eq. (18) when $l = 0$, the only difference being the form of the base flow and the boundary condition $\hat{T} = 0$ at the endpoints. Table 2 shows excellent agreement between the values of the critical Rayleigh number Ra_c calculated by Bergholz using from 24 to 30 eigenfunctions and by us using $N = 80$ or $N = 100$ computational points.

5. Results

The validity of the parallel flow approximation in a finite cavity may be established for different values of q, by solving numerically the full set of governing equations (2)–(4), at moderate Rayleigh numbers. Initial test calculations are carried out for $Ra = 10^5$ and $Pr = 1$ with

Table 2
Predicted $Ra_c \times 10^{-3}$ previous Galerkin method and present finite-difference approach

Pr	γ	Bergholz	Present $N = 60$	Present $N = 80$	Present $N = 100$
0.73	6.0	134.77	137.25	136.10	135.59
5.0	3.0	57.95	58.11	58.04	58.00
5.0	8.0	163.55	161.85	162.61	162.94
12.7	1.0	87.50	86.88	87.17	87.30
12.7	7.0	128.14	127.14	127.57	127.75

fully implicit time discretization, using the power-law scheme of Patankar [17] for spatial discretization by control volumes, which is adequate for a flow of this type.

The parallel character of the base flow over the central region of the cavity is verified in Fig. 4 for $A \geqslant 4$ or so when $q = 1$ whereas aspect ratios of the order of 9 are required for $q = 10$. The subsequent plots in Fig. 5 of $\Psi(0)$ versus Ra obtained from Eq. (9), which is strictly valid only for a cavity extending to infinity along y, are also in good agreement with the numerical maxima for an aspect ratio $A = 5$ and confirm the validity of the parallel approximation for small values of q. As Ra increases, however, the influence of the top and bottom ends of the cavity on the flow pattern becomes more important and the agreement between theory and numerical solution is not as close as for the lower Ra values.

Preliminary calculations with the eigenvalue problem equation (18) reveal that two-dimensional disturbances propagating along the y-direction are the most unstable only for small Prandtl numbers. The critical disturbances are otherwise three-dimensional for any other value of Pr, propagating at some angle β in the (y–z) plane. The purpose of this angle is to define the direction of propagation in such a way that $k = \tilde{k}\cos\beta$ and $l = \tilde{k}\sin\beta$. Consequently, the discussion of the stability results to follow is better done in terms of $\tilde{k}$ and β instead of k and l.

From a general point of view, it can be expected that the physical origin of the instabilities will be different, depending on the value of Pr. Either hydrodynamic modes, due to a destabilization of the velocity profile, or thermal modes, due to a destabilization of the temperature profile will occur first. If $Pr < 1$, thermal diffusivity is greater than viscous diffusivity and thermal disturbances of the base flow are prone to be dissipated faster than hydrodynamic disturbances. Clearly, the instabilities are then most likely to be caused by hydrodynamic

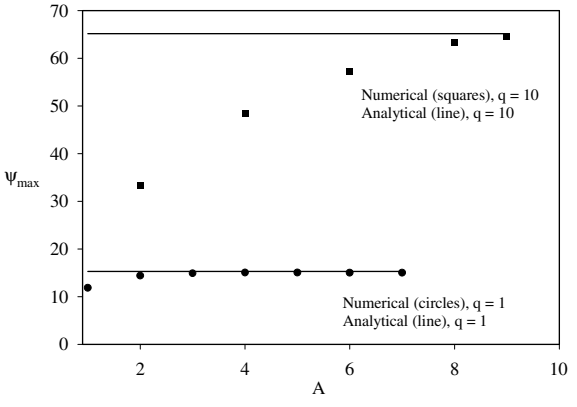

Fig. 4. Streamfunction maximum vs A, $Pr = 1$.

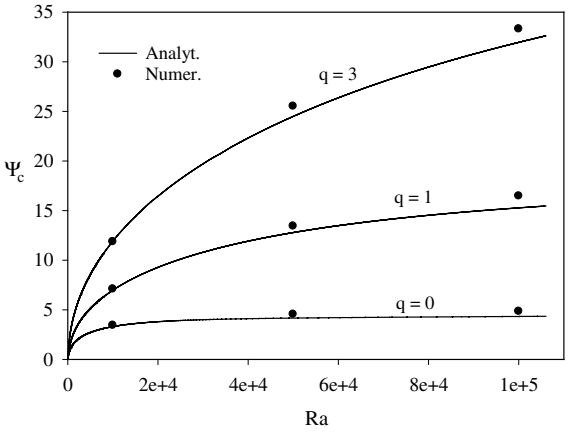

Fig. 5. Streamfunction maximum vs Ra for $Pr = 1$, $q = 0$, 1, 3.

disturbances gaining energy from the base flow by the action of shear. On the other hand, as Pr increases, thermal disturbances are expected to be at the origin of the main mode of instabilities.

Solutions of the eigenvalue problem equation (18) also reveal that σ_i is always different from zero on the stability curves, on which $\sigma_r = 0$ by definition. This indicates a Hopf bifurcation of the base flow solution, characterized by oscillating instability modes. Unlike what was found [12,13] in the case of a vertical cavity with a fixed temperature difference imposed between the walls, oscillating instabilities are predicted over the entire range of parameters Ra, Pr and q considered in the present study. Fig. 6 displays the marginal stability curves along the critical direction β_c for $Pr = 1$ and different values of q. It is noticed that there is only one minimum in the stability curve for $q = 1$ or 2 while the curve for $q = 10$ has two branches and displays not one, but two minima. Each minimum indicates the critical Rayleigh number for a different mode of instability, driven by different physical mechanisms.

Some insight on the physical significance of the different modes of instability can be gained from the kinetic and thermal potential energy balances of the disturbances. Multiplying the first equation of the eigenvalue problem system equation (18) by $\hat{u}^*$, the second one by $\hat{v}^*$, the last one by $\hat{T}^*$, integrating from $x = -1/2$ to $x = 1/2$ and taking the real part of the results gives, after a few rearrangements

$$\begin{aligned} \sigma_r E_{kin} &= -Pr\dot{E}_{vis} + \dot{E}_U + RaPr\dot{E}_b \\ \sigma_r E_{pot} &= -\dot{E}_{dif} - \alpha\dot{E}_b + \dot{E}_T \end{aligned} \tag{19}$$

for the rates of change of the disturbance kinetic energy E_{kin} and thermal potential energy E_{pot} defined in Appendix A along with all the other terms in Eq. (19). The first terms on the right-hand side $-Pr\dot{E}_{vis}$ and $-\dot{E}_{dif}$, always negative, account for the rates of loss of kinetic

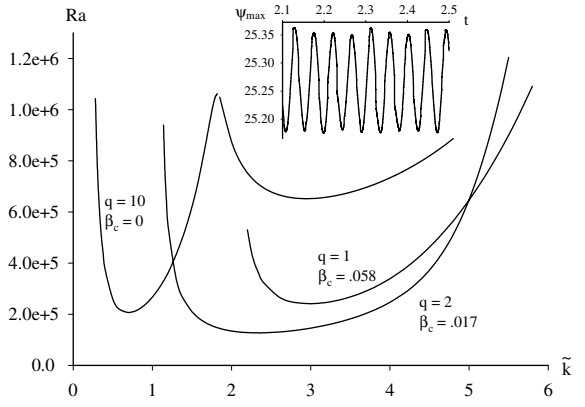

Fig. 6. Marginal stability at critical β for $Pr = 1$, $q = 1$, 2, 10.

energy due to viscous dissipation and loss of potential energy due to heat diffusion, respectively. In the remaining terms, $\dot{E}_U$ is the rate of kinetic energy transfer from the base flow, $RaPr\dot{E}_b$ is the rate of change of kinetic energy caused by buoyancy while $-\alpha\dot{E}_b$ represents the rate of change of potential energy related to stratification. Finally, $\dot{E}_T$ is the rate of change of potential energy associated with the interactions of the disturbance with the horizontal base flow temperature gradient.

The relative values for the various terms entering the energy balances Eq. (19), computed using $N = 90$, are displayed in Table 3 for $q = 10$, at critical points for several Prandtl numbers. Normalization of the data is done in such a way that $-Pr\dot{E}_{vis} = -1$ and $-\dot{E}_{dif} = -1$. Therefore the sum of the normalized $\dot{E}_U$ and $RaPr\dot{E}_b$ values, as well as that of the normalized $-\alpha\dot{E}_b$ and $\dot{E}_T$, should be equal to one in principle on the stability curve. The fact that they are indeed very close to unity is also a good indicator that the solutions are correct. One can see from the data that the disturbance derives the bulk of its kinetic energy from the buoyancy term in every case but one. Hence, instability is normally buoyancy-driven except for Pr values smaller than one, in which case it can be shear-driven from the mean flow. Going back to Fig. 6, the conclusion is that thermal instability is the preferred instability mode for $q = 10$ and $Pr = 1$. The other minimum gives the critical Rayleigh number for the hydrodynamic mode, characterized by higher wavenumber wavelength and faster oscillations. For the lower heat flux ratio values $q = 1$ and 2, only critical Rayleigh numbers for thermal instability are found.

Also shown on Fig. 6 are the oscillations in the maximum stream function value of the numerical solution of Eqs. (2)–(4), obtained in a cavity of aspect ratio $A = 5.4$ from the same computer code used earlier to simulate the base flow. The small oscillations were detected using a 25 by 121 grid mesh and a time step $\Delta t = 10^{-4}$ for $q = 2$, $Pr = 1$ and a Rayleigh number $Ra = 1.15 \times 10^5$, which is close to the theoretical prediction $Ra_c = 1.27 \times 10^5$ for the thermal mode. The frequency of oscillation $\omega \approx 140$ of the numerical solution is also of the same order as the theoretical value $\omega_c = 200.4$.

The transition from a shear-driven to a buoyancy-driven instability under the influence of the Prandtl number can be appreciated in Fig. 7, where marginal stability curves are shown for $q = 10$. It is clear from the plots that the critical Rayleigh number corresponds to the hydrodynamic instability mode for $Pr = 0.3$ and to the thermal instability mode for $Pr = 1.0$. Only one minimum is found on the graph for $Pr = 7$, associated with the thermal instability mode. It can be noticed that the critical Rayleigh number is reduced as the Prandtl number increases from small values. The initial influence of the parameter Pr is thus a destabilizing one.

A better global picture is provided by Fig. 8, showing the critical Rayleigh number Ra_c versus the Prandtl number for different values of q. The conclusion is that the base flow is much more stable for both very small and rather large Prandtl numbers than for Pr values of the order of, say, one. This is related to the stronger viscous damping of velocity disturbances for large Pr values and the quicker dissipation of temperature disturbances by thermal diffusion for low Pr values. The stabilizing influence of the Prandtl number within the higher range of values is more or less pronounced depending on the value of the heat flux ratio q, however. The latter has an influence on the base flow solution itself, and consequently on the stability of the flow. It is found from Fig. 8, not surprisingly, that Ra_c increases as q becomes smaller, since instabilities are known to occur at very large Ra for a cavity heated sideways.

Table 3
Relative values of terms in disturbance energy balances equation (19) for $q = 10$

Pr	$\tilde{k}_c$	$\dot{E}_U/Pr\dot{E}_{vis}$	$Ra\dot{E}_b/\dot{E}_{vis}$	$-\alpha\dot{E}_b/\dot{E}_{dif}$	$\dot{E}_T/\dot{E}_{dif}$
50	2.621	0.0419	0.9576	−0.1241	1.1224
10	1.909	0.1527	0.8431	−0.1221	1.1207
1	0.697	0.0992	0.9011	−0.1404	1.1393
0.441	0.483	0.3539	0.6459	−0.1283	1.1276
0.441	1.633	1.2695	−0.2708	0.3186	0.6828

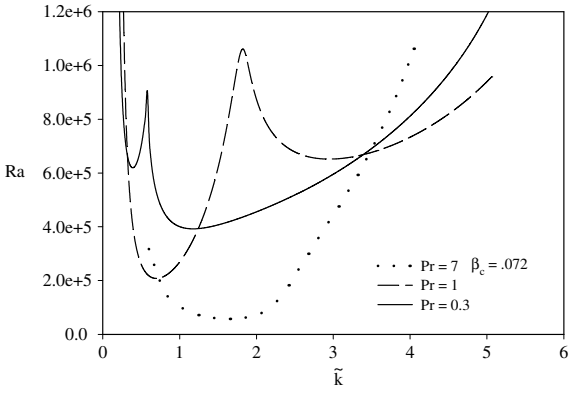

Fig. 7. Marginal stability at critical β for $q = 10$, $Pr = 0.3$, 1, 7.

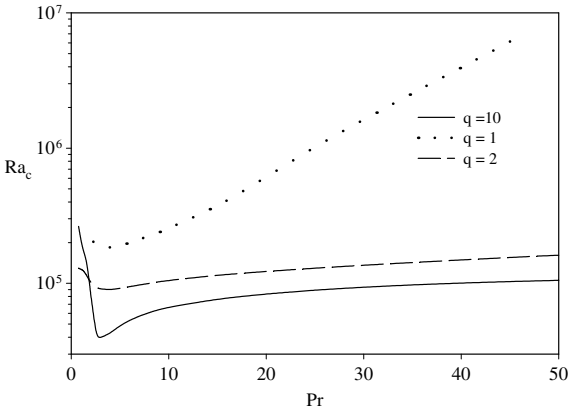

Fig. 8. Critical Rayleigh number vs Pr.

Fig. 9 shows the direction of propagation β_c of the critical disturbance, versus Pr, for several values of q. It is clear from the plot that two-dimensional disturbances in the (x, y) plane are the most unstable only for small Prandtl numbers. For Prandtl numbers greater than 0.75 or 1, the critical disturbance involves a transverse velocity component along z. Fig. 10 shows that the critical wavenumber k_c increases monotonically with Pr toward asymptotic values for $q = 2$ and 10. We can also observe that smaller values of k_c are found for larger values of q, or equivalently, that the wavelength of the secondary flow cells increase with q. The oscillation frequency $\omega_c = \sigma_i$ of the instability cells is also shown in Fig. 11. The frequency is seen to increase with Pr for $q = 1$ and to level out in the other cases.

The question naturally arises as to whether both buoyancy and shear driven instabilities can occur at the same critical Rayleigh number for a given heat flux ratio q. This is indeed the case for low Prandtl numbers. Equivalently, the two instability modes can share the same critical Rayleigh numbers at some q for a given Pr.

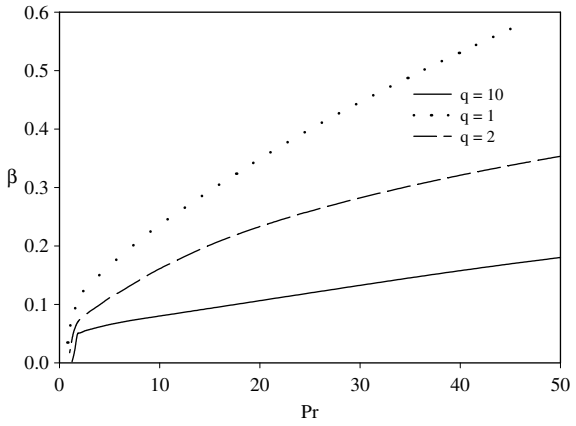

Fig. 9. Critical direction of propagation β_c vs Pr.

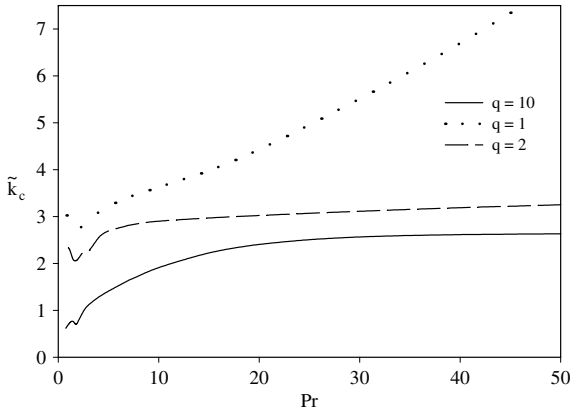

Fig. 10. Critical wavenumber vector modulus $\tilde{k}_c$ vs Pr.

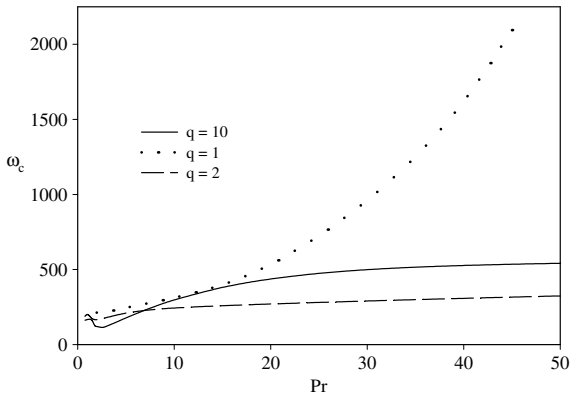

Fig. 11. Critical oscillation frequency ω_c vs Pr.

This situation corresponds to a point of intersection of the hydrodynamic and thermal marginal stability curves

in a (Pr, Ra) or (q, Ra) plane, called a codimension two point [19]. For $q = 10$, the codimension point is located at $Pr = 0.441$, and the common critical Rayleigh number for thermal and hydrodynamic modes has the value $Ra_c = 4.22 \times 10^5$. Terms of the disturbance energy balances are provided for each mode in Table 3. Streamlines and isotherms are represented in Fig. 12, without the time-dependence, for each respective type of disturbance. There are numerous qualitative differences between the thermal and hydrodynamic modes. One of the most striking features of the thermal mode being the much longer cells and greater symmetry of the streamlines.

The Rayleigh number at the codimension point is found to increase almost linearly with q, from a value of $Ra_c = 2.087 \times 10^5$ when $q = 3$ to a value of $Ra_c = 4.199 \times 10^5$ when $q = 10$. At the codimension points, the values of the critical parameters k and ω are always higher for the hydrodynamic mode than for the thermal mode, but vary otherwise in the same way with respect to q. The wavenumber k decreases slowly, while the oscillation frequency increases slightly. In a (q, Pr) plane, the codimension points define a curve $Pr(q)$ representing the borderline between the thermal (above) and hydrodynamic (below) modes as shown in Fig. 13 which summarizes what type of instability will occur for given values of the parameters q and Pr, according to the linear stability theory.

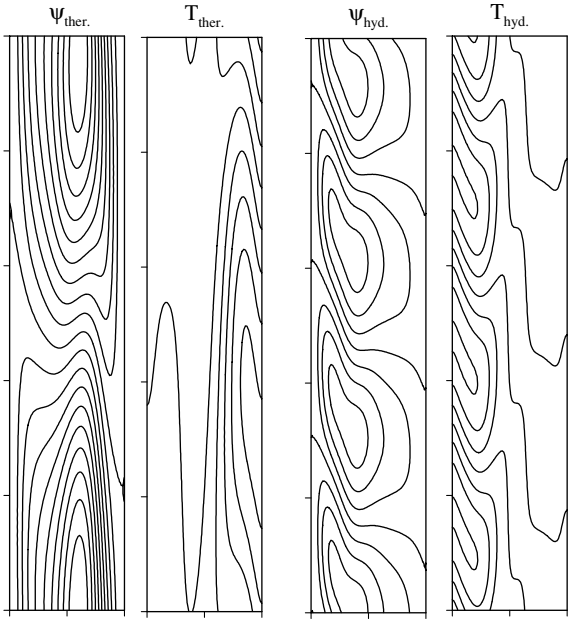

Fig. 12. Streamlines and isotherms for thermal and hydrodynamic disturbances. $Ra = 4.220 \times 10^5$, $q = 10$, $Pr = 0.441$.

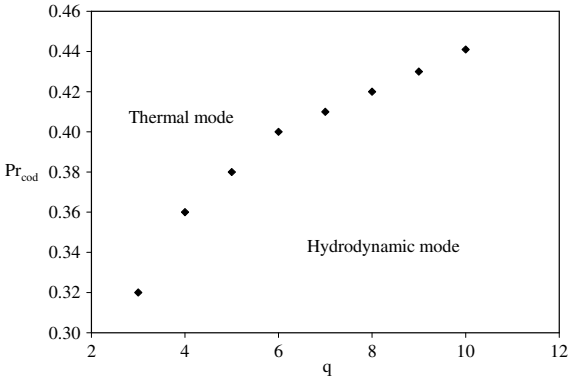

Fig. 13. Prandtl number value at codimension point vs q.

6. Conclusion

The linear stability of parallel, free convection flow within a tall vertical cavity submitted to crossed uniform heat flux conditions on the boundaries has been examined. It is found that for stable stratification of the base flow, three-dimensional instabilities will occur in general. These instabilities are always oscillating, in contrast with what is found when a constant temperature difference is imposed on the vertical walls. It is found that shear-driven instabilities can occur for $Pr < 1$, but that otherwise buoyancy-driven instabilities are predicted. For small Prandtl numbers, both instability modes can occur at the same time for a given heat flux ratio and two-dimensional disturbances propagating along the vertical axis can be critical.

Acknowledgement

This research was supported by the Natural Sciences and Engineering Research Council of Canada.

Appendix A

The various quantities appearing in the disturbance energy balances equation (19) are defined as follows:

$$E_{\mathrm{kin}} = \frac{1}{2}\int_{-1/2}^{1/2} |\hat{u}|^2 + |\hat{v}|^2 + |\hat{w}|^2 \,\mathrm{d}x$$

$$E_{\mathrm{pot}} = \frac{1}{2}\int_{-1/2}^{1/2} |\hat{T}|^2 \,\mathrm{d}x$$

$$\dot{E}_{\mathrm{vis}} = \frac{1}{2}\int_{-1/2}^{1/2} \tilde{k}^2(|\hat{u}|^2 + |\hat{v}|^2 + |\hat{w}|^2) + |\hat{u}'|^2 + |\hat{v}'|^2 + |\hat{w}'|^2 \,\mathrm{d}x$$

$$\dot{E}_{\mathrm{dif}} = \frac{1}{2}\int_{-1/2}^{1/2} |\hat{T}'|^2 + \tilde{k}^2|\hat{T}|^2\,\mathrm{d}x$$

$$\dot{E}_{\mathrm{U}} = \frac{1}{2}\int_{-1/2}^{1/2} \psi'' \mathrm{Re}(\hat{u}\hat{v}^*)\,\mathrm{d}x$$

$$\dot{E}_{\mathrm{B}} = \frac{1}{2}\int_{-1/2}^{1/2} \mathrm{Re}(\hat{v}^*\hat{T})\,\mathrm{d}x$$

$$\dot{E}_{\mathrm{T}} = -\frac{1}{2}\int_{-1/2}^{1/2} \theta' \mathrm{Re}(\hat{u}\hat{T}^*)\,\mathrm{d}x$$

References

[1] A. Bejan, The boundary layer regime in a porous layer with uniform heat flux from the side, Int. J. Heat Mass Transfer 26 (1983) 1339–1346.

[2] D.E. Cormack, L.G. Leal, J. Imberger, Natural convection in a shallow cavity with differentially heated end walls, part 1. Asymptotic theory, J. Fluid Mech. 65 (1974) 209–229.

[3] D.E. Cormack, L.G. Leal, J.H. Seinfeld, Natural convection in a shallow cavity with differentially heated end walls, part 2, Numerical solutions, J. Fluid Mech. 65 (1974) 231–246.

[4] J. Imberger, Natural convection in a shallow cavity with differentially heated end walls, part 3, Experimental results, J. Fluid Mech. 65 (1974) 247–260.

[5] A. Bejan, C.L. Tien, Laminar natural convection heat transfer in a horizontal cavity with different end temperatures, J. Heat Transfer 100 (1978) 641–647.

[6] D.R. Kassoy, B. Cotte, The effects of sidewall heat loss on convection in a saturated porous vertical slab, J. Fluid Mech. 152 (1985) 361–378.

[7] M. Wang, D.R. Kassoy, P.D. Weidman, Onset of convection in a vertical slab of porous media between two impermeable conducting blocks, Int. J. Heat Mass Transfer 30 (1987) 1331–1341.

[8] P. Vasseur, M.G. Satish, L. Robillard, Natural convection in a thin inclined porous layer exposed to a constant heat flux, Int. J. Heat Mass Transfer 30 (1987) 537–549.

[9] M. Sen, P. Vasseur, L. Robillard, Multiple steady states for unicellular natural convection in an inclined porous layer, Int. J. Heat Mass Transfer 30 (1987) 2097–2113.

[10] D.A. Nield, Convection in a porous medium with inclined temperature gradient, Int. J. Heat Mass Transfer 34 (1991) 87–92.

[11] S. Kimura, M. Vynnycky, F. Alavyoon, Unicellular natural circulation in a shallow horizontal porous layer heated from below by a constant flux, J. Fluid Mech. 294 (1995) 231–257.

[12] S.A Korpela, D. Gözüm, C.B. Baxiç, On the stability of the conduction regime of natural convection in a vertical slot, Int. J. Heat Mass Transfer 16 (1973) 1683–1690.

[13] R.F. Bergholz, Instability of steady natural convection in a vertical fluid layer, J. Fluid Mech. 84 (1978) 743–768.

[14] S.A. Suslov, S. Paolucci, Stability of natural convection flow in a tall vertical enclosure under non-Boussinesq conditions, Int. J. Heat Mass Transfer 38 (1995) 2143–2157.

[15] A. Bahloul, I. Mutabazi, A. Ambari, Codimension 2 points in the flow inside a cylindrical annulus with a radial temperature gradient, Eur. Phys. J. 9 (2000) 253–264.

[16] D.D. Gray, A. Giorgini, The validity of the Boussinesq approximation for liquids and gases, Int. J. Heat Mass Transfer 19 (1976) 545–551.

[17] S.V. Patankar, Numerical Heat Transfer and Fluid Flow, McGraw-Hill, 1980.

[18] P.G. Drazin, W.H. Reid, Hydrodynamic Stability, Cambridge University Press, 1991.

[19] P. Chossat, G. Iooss, The Couette–Taylor Problem, Springer-Verlag, 1994.